

ORIGINAL RESEARCH

Seismic Performance Enhancement of Heritage Adobe Vaults in Machi Windcatchers Using FRP and Steel Rebars: A Nonlinear Dynamic Study Based on ABAQUS Modeling

Shahraki M.^{1*} Agha Kasiri sh²

Abstract:

The traditional adobe windcatcher structures (Āsbaads) of Sistan, Iran, represent a unique form of vernacular architecture that is currently under consideration for UNESCO World Heritage inscription. Despite their historical and cultural significance, these arched vaults suffer from serious structural vulnerabilities due to material degradation and lack of reinforcement, especially under seismic loading. This research addresses the urgent need for preserving such heritage by assessing the seismic performance of adobe vaults in the Qaleh Machi windmills, Iran with a focus on enhancing their resilience through modern retrofitting techniques. The study employs a series of nonlinear dynamic time-history analyses using calibrated finite element models developed in ABAQUS 2020. Both unreinforced and retrofitted configurations were modeled under three strong-motion earthquake records: Sarpol-e Zahab, Tabas, and Northridge. Two retrofitting systems—traditional steel rebars and Fiber Reinforced Polymer (FRP) bars were implemented using the Near-Surface Mounted (NSM) technique. Mesh sensitivity analysis, material calibration based on laboratory tests, and realistic boundary conditions were incorporated to ensure high-fidelity simulation results. The findings reveal that FRP-retrofitted vaults consistently outperformed their unreinforced and steel-reinforced counterparts, achieving up to 54% reduction in peak displacement and 48% in plastic strain. Moreover, FRP strengthening significantly improved energy dissipation, delayed stiffness degradation, and enhanced ductile behavior under cyclic loading. These results underscore the effectiveness of advanced composite retrofitting as a structurally robust and culturally appropriate solution for conserving adobe heritage in seismically active regions.

Keywords:

Seismic Performance, FRP, ABAQUS, Nonlinear Dynamic Study

✉*Corresponding author Email: Mehdi.shahraki@iau.ac.ir

1. Department of Civil Engineering, Zah.C., Islamic Azad University, Zahedan, Iran

2. Department of Civil Engineering, TS.C., Islamic Azad University, Tehran, Iran. Sh.aghakasiri@aiu.ir

1. Introduction

Many arches in adobe windmills across the world have suffered serious deterioration due to exposure to sulfates, chlorides, and other aggressive agents. This phenomenon has led to significant expenses related to the repair, rehabilitation, or even complete replacement of damaged arches in such traditional structures. In many cases, the implications extend beyond an engineering challenge and are perceived as a serious socio-economic issue. The repair and replacement of damaged adobe arches have imposed millions of dollars in financial losses globally [1].

For centuries, Iranians have constructed various types of windmills tailored to their climatic conditions to grind wheat and other grains an essential step in daily bread production, which constituted a staple food. Although these historical structures once played a vital role in daily life, their use has declined with the rise of industrial and technological advancements. Nevertheless, they embody significant architectural and engineering characteristics that reflect ancestral wisdom in adapting to environmental and climatic conditions. Sistan is regarded as the original cradle of these windmills. Moreover, the windmills of Sistan and South Khorasan are currently candidates for inscription on the UNESCO World Heritage List. The arches embedded in these windmills are among the most prominent features of Iranian architectural heritage.

Unfortunately, no comprehensive studies have been conducted so far on the seismic strengthening of these arches or windmills, despite the fact that Iran lies in a highly seismically active zone. To date, only superficial restoration measures have been undertaken, with no rigorous research addressing preemptive retrofitting strategies. This study, therefore, focuses on the seismic analysis of both flat and vaulted arches in the adobe windcatcher structures (*Āsbaads*) of Sistan, Iran of Qal'eh Machi, Iran and their strengthening using modern methods. In

particular, the study evaluates the application of Fiber Reinforced Polymers (FRP) as an alternative to traditional steel reinforcement bars for improved seismic resilience.

In a study conducted by Hu et al. [2], it was found that adobe vaults particularly those constructed prior to 1970—often lack sufficient reinforcement within their core or along the lateral supports for longitudinal steel bars. Confined vaults exhibited brittle behavior with limited deformation capacity. When subjected to increased loads, degradation, or cyclic loading conditions—whether due to aging or retrofitting—additional reinforcement may be necessary, provided that it meets the required force and ductility demands. In recent years, advanced composite materials have been increasingly utilized to retrofit adobe vaults in seismically active regions. A considerable body of research has focused on using polymer-based or plastic fiber materials for strengthening earthen structures.

Building on the extensive body of research utilizing advanced composite materials and nonlinear modeling for seismic strengthening of adobe vaults, recent studies have focused on integrating energy-dissipative and self-centering mechanisms into structural systems. Garmeh et al. [3] proposed an innovative self-centering eccentrically braced frame (SC-EBF) incorporating Shape Memory Alloy (SMA) bolts and a vertically oriented link. Their finite element simulations in ABAQUS demonstrated a significant reduction in residual displacements and stable hysteresis performance under cyclic loading. This approach underscores the importance of incorporating material-based adaptive features, such as SMA, to enhance seismic energy dissipation and post-event functionality.

Complementary to this direction, Arezoomand et al. [4] investigated the influence of design optimality and over strength on the seismic performance of steel plate shear walls (SPSWs). Their findings revealed that design detailing and post-

buckling behavior substantially affect collapse capacity and fragility profiles. Furthermore, their subsequent work [5] compared approximate pushover-to-fragility methodologies with exact incremental dynamic analyses for SPSWs, highlighting key limitations and efficiencies in seismic assessment practices. Though focused on steel systems, these insights on fragility, over strength, and deformation demand bear direct relevance to the present study's approach in modeling the seismic resilience of heritage adobe arches.

Toutanji and Balaguru [6] presented the results of a laboratory investigation evaluating the performance of large-scale adobe specimens confined using composite rebars made of FRP and GFRP sheets. The experimental program was conducted under three environmental conditions at room temperature: humidity, dryness, and freeze exposure. The test results revealed that under both humid and dry conditions, FRP-confined samples did not show significant reductions in strength or ductility. However, GFRP-confined samples exhibited noticeable performance degradation under the same conditions. In the freeze exposure scenario, both FRP and GFRP specimens experienced considerable declines in strength and ductility. Most of the previous studies have focused on circular adobe vaults subjected to concentric loading. Nevertheless, in practical applications, it is uncommon for adobe vaults to be subjected solely to purely concentric loads.

Boury et al. [7] investigated the effectiveness of an innovative method for strengthening masonry arches on their intrados using carbon plates. Although FRP sheets or strips have been successfully used as strengthening elements in such applications, this study examined fifteen brick arch specimens internally retrofitted with either GFRP sheets or CFRP plates. These specimens were tested under a uniformly distributed vertical load applied at the keystone. The research explored the influence of the type of reinforcement (glass fibers vs. carbon plates), the properties

of the bond system and masonry substrate, and the presence of anchorage clusters.

Dimitri and Trentinabin [8] conducted a numerical study to understand the stability of unreinforced masonry arches and portals. The analytical model's predictions were compared with results from numerical simulations using the Discrete Element Method (DEM). In this numerical model, the masonry was idealized as a collection of rigid blocks connected through frictional interfaces without tensile strength, based on a step-by-step integration of the motion equations for each block. A satisfactory correlation between analytical and numerical results confirmed the validity of the analytical model and validated the proposed approach for assessing the quasi-static behavior of unreinforced masonry structures.

Carozzi et al. [9] presented a finite element-based analysis program suitable for predicting failure mechanisms, thrust lines, and collapse behavior both in the presence and absence of TRM, SRG, and FRP reinforcements. This method employed quadrilateral discretization of the masonry and incorporated interfaces between adjacent elements with limited strength, modeled as continuous plastic trusses. The results demonstrated that strengthening significantly increased the structural lifespan, and carbon fibers proved to be both cost-effective and structurally efficient as reinforcement materials. Button and Karnin [10] studied the influence of the vertical component of seismic action on six masonry arches with various static support configurations. Their research included linear spectral analyses and both linear and nonlinear time-history analyses. Based on their findings, they provided recommendations on the specific conditions under which the vertical seismic component should be considered and proposed methods for integrating this effect into seismic load combinations.

A comprehensive multi-hazard reliability assessment was recently conducted by Pouraminian et al. [11] on a historic brick minaret located in Gaskar, Iran, focusing on its performance under combined seismic and

wind actions. To accurately simulate the structural response, the study employed advanced finite element modeling techniques in conjunction with national building code provisions. The authors utilized Monte Carlo simulations as part of their probabilistic framework to quantify the safety margins of the structure under different loading scenarios. Their findings revealed that while the minaret demonstrated acceptable performance under design-level wind forces, it exhibited significant vulnerability when subjected to seismic excitations.

As previously observed, several studies have focused on the static and axial loading behavior of stone and adobe arches through laboratory experiments and finite element modeling. However, no comprehensive research has yet been conducted on the nonlinear dynamic time-history analysis of these traditional windmill arches, particularly those located in the Sistan region, using strong-motion earthquake records from both global and Iranian databases. This research gap becomes more pronounced as many of these historical structures continue to deteriorate over time. In the present study, the seismic retrofitting of the ancient arched structures of the Qal'eh Machi, Iran windmills is investigated. Fragility and vulnerability curves are derived for the targeted arch based on nonlinear dynamic analyses, followed by the evaluation of a resilience index reflecting the extent of seismic-induced damage.

2. Theoretical Framework

2.1. Architectural Characteristics of the Qaleh-Machi Windmills, Iran

These historical structures are located within the Hosehdar archaeological zone, situated in the southeastern quadrant of the Qaleh-Machi fortress. The windmills occupy a plot of land measuring approximately 3,300 square meters, with the estimated spatial footprint of each structure being 30×30 meters. The actual dimensions of the individual windmills are approximately 9.5 by 7 meters, resulting in a footprint of about 66.5 square meters.

Constructed on a platform raised 40 centimeters above the surrounding terrain, each windmill reaches a total elevation of 80.6 centimeters from the base. The roofs are either domed or flat, and are finished using mud-straw plaster as illustrated in Figure 1 and Figure 2.

Each windmill includes a single southern entrance, and the wall thickness reaches up to one meter. Notably, there are no decorative elements observed within these structures. The primary construction materials consist of sun-dried adobe bricks and mud-straw mortar, while fired bricks were employed for the exterior flooring. Architectural floor plans for the windmills are presented in Figures 3 and 4.

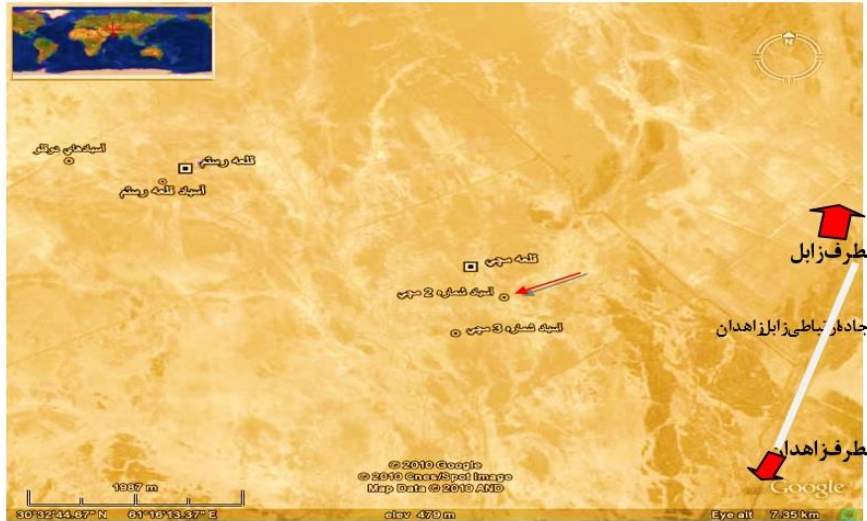
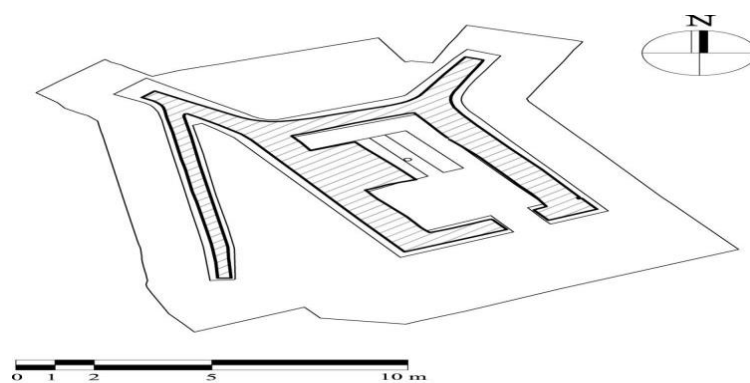


Fig. 1. Location of the adobe windcatcher structures (Āsbaads) of Sistan, Iran within the historical district of Howz-e-Dar



Fig. 2. Northern and Southern Elevation Views of Windmill No. 2 After Restoration



Level 2 : 1.27 m

Fig. 3. Plan view taken at an elevation of 1.27 meter from the base of the adobe windcatcher structures (Āsbaads) of Sistan, Iran, featuring an arched vault structure

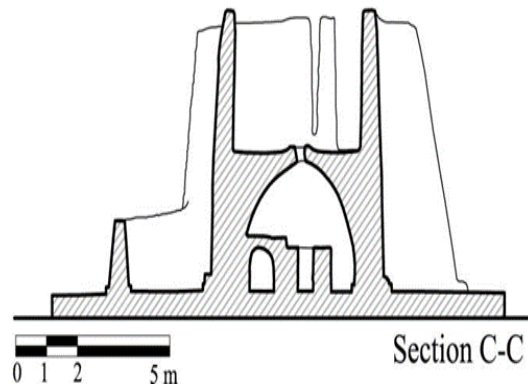


Fig. 4. Cross-section of adobe windcatcher structures (Āsbaads) of Sistan, Iran with vaults arched (scale 1:200)

To evaluate the material properties of the adobe and mortar used in the vaults, a representative sample was collected from the Asbad (windmill) structure located in Qaleh Mouchi, Iran. The specimen was sent to a geotechnical laboratory for uniaxial compressive strength testing of the soil, following the ASTM D2166 standard protocol. The results of these tests for each

sample are presented in Table 1. The mechanical and geometrical specifications of the steel reinforcement bars and the Fiber Reinforced Polymer (FRP) bars utilized in this study are provided in Table 2. Furthermore, the characteristics of the examined vaults, modeled under different configurations, are summarized in Table 3.

Table 1. Material Properties of Mudbrick and Mortar Used in the Domed Roof of the Qaleh Machi Windmill, Iran

Sample Description	Elastic Modulus (E_1) (MPa)	Tensile Strength (X_{\square}) (MPa)	Compressive Strength (X_c) (MPa)	Moisture Content (%)	Failure Strain (%)
3.81 × 7.61					
Mortar	1391	1.7	10.8	1.0	1.2
Mudbrick	1776	1.4	8.9	0.7	1.0

Table 2. Mechanical and Physical Properties of FRP and Steel Reinforcement Bars [9]

Property	FRP Rebar	Steel Rebar
Specific gravity	7.1	9.7
Yield strength (MPa)	701	600
Ultimate strength (MPa)	483	380
Compressive strength (MPa)	310 – 482	380
Tensile modulus (GPa)	55	200
Coefficient of thermal expansion	9.9	7.11

Table 3. Model Specifications Based on Geometry, Retrofitting Technique, and Earthquake Record

Model ID	Vault Geometry	Retrofitting Type	Earthquake Record	Time
A-S-1	Vaulted	Unretrofitted	Sarpol-e Zahab	2017
A-S-2	Vaulted	Retrofitted with Steel Rebar	Sarpol-e Zahab	2017
A-S-3	Vaulted	Retrofitted with FRP Rebar	Sarpol-e Zahab	2017
A-T-1	Vaulted	Unretrofitted	Tabas	1978
A-T-2	Vaulted	Retrofitted with Steel Rebar	Tabas	1978
A-T-3	Vaulted	Retrofitted with FRP Rebar	Tabas	1978
A-N-1	Vaulted	Unretrofitted	Northridge	1994
A-N-2	Vaulted	Retrofitted with Steel Rebar	Northridge	1994
A-N-3	Vaulted	Retrofitted with FRP Rebar	Northridge	1994

2.2. Evaluation of Earthquake Records

To perform a time history dynamic analysis on the studied vault structure, ground motion records from major global earthquakes as well as one significant seismic event in Iran were utilized. These records were retrieved from

the Pacific Earthquake Engineering Research Center (PEER) ground motion database. The selected ground motions correspond to the Sarpol-e Zahab, Tabas, and Northridge earthquakes, as illustrated in Figures 5 through 7.

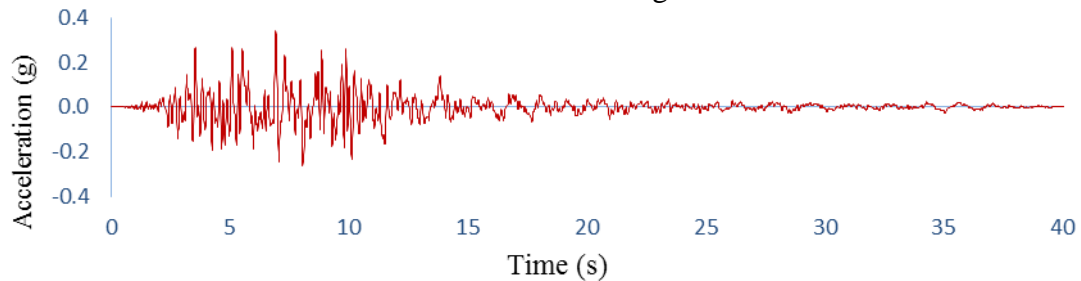


Fig. 5. The Horizontal Component of the Sarpol-e Zahab Earthquake Record (2017)

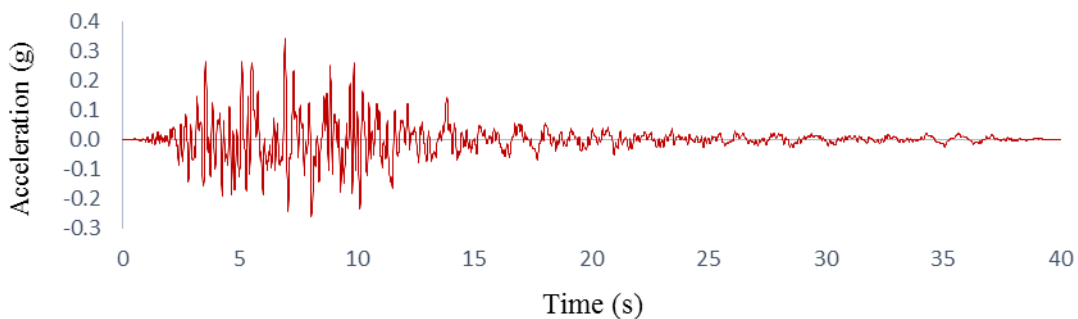


Fig. 6. The Horizontal Component of the Tabas Earthquake Record (1978)

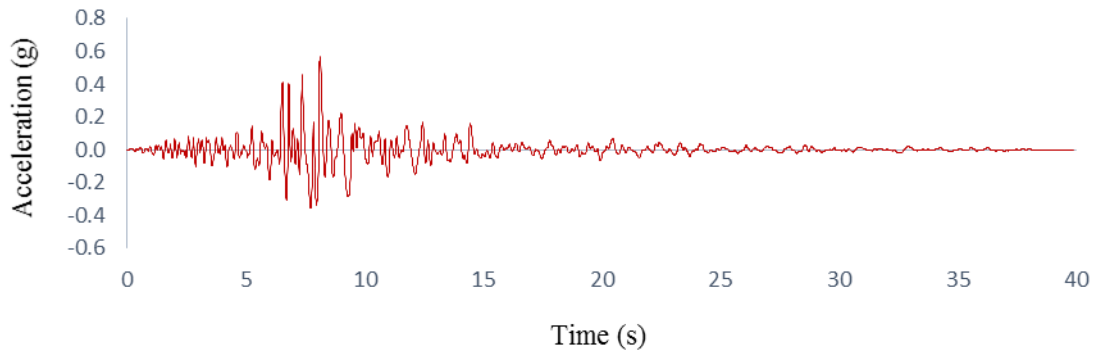


Fig. 7. The Horizontal Component of the Northridge Earthquake Record (1994)

The characteristics of the selected ground motion records are presented in Table 5, respectively.

As illustrated, the selected ground motion records cover a broad range of frequency content and seismic acceleration amplitudes. While these records may exceed the minimum design requirements particularly those specified in the Iranian Seismic Code (Standard No. 2800), which mandates that the duration of strong ground motion be at least 10 seconds or three times the fundamental period of the structure, whichever is greater they were deliberately chosen for this study. This selection is justified by the research objective, which focuses on evaluating the seismic performance of a defective adobe

arch and its retrofitting under various earthquake scenarios.

The combined response spectra obtained within the period range of $0.2T$ to $1.5T$ were compared with the standard design spectrum. The scale factor was determined in such a way that, throughout this range, the average spectral values never fell below 1.17 times the corresponding values of the design spectrum. The calculated scale factors were then applied to the selected ground motion records, and the scaled records were subsequently used as input for time-history analysis. Figure 8 illustrates the combined response spectra of the three selected earthquakes, prepared for import into the analysis software.

Table 4. Characteristics of Selected Ground Motion Records

Ground Motion Record	Peak Ground Acceleration (g)	Peak Ground Velocity (cm/s)	Peak Ground Displacement (cm)
Sarpol-e Zahab	0.432	45.677	9.043
Tabas	0.854	98.949	37.527
Northridge	0.568	51.826	9.034

Table 5. Summary of the Seismic Parameters of the Selected Earthquakes

Parameter	Sarpol-e Zahab Earthquake – Iran	Tabas Earthquake – Iran	Northridge Earthquake – USA
Moment Magnitude (Mw)	7.3	7.8	7.3
Local Date and Time of Occurrence	November 12, 2017 – 21:48:16	September 16, 1978 – 15:35:56	January 17, 1994 – 12:30:55
Epicenter Longitude (°)	45.9 E	40.57 E	118.517 W
Epicenter Latitude (°)	34.84 N	35.33 N	34.312 N
Hypocentral Depth (km)	11	5	11.4

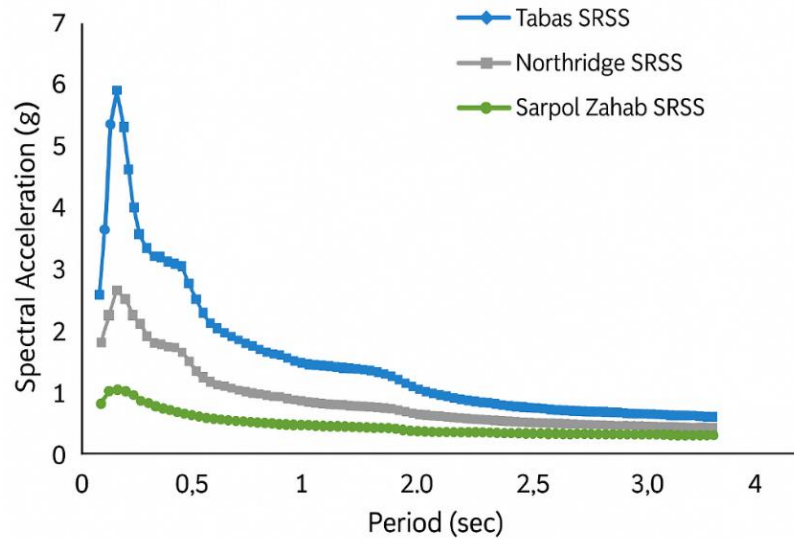


Fig. 8. Combined and Non-Directional Response Spectrum (Square Root of the Sum of Squares) of the Three Selected Earthquakes

3. Methodology

3.1. Numerical Study

A detailed investigation conducted by Morshedi et al. [13] explored the influence of retrofitting on adobe masonry arch bridges. In their study, a full-scale (1:1) stone-arch specimen was tested under concurrent vertical and lateral loading conditions using ABAQUS 2020, as illustrated in Figure 3. The vertical loads were introduced through the spring element placed on the impost, followed sequentially by lateral loads acting on the arch span. In the initial test scenario, the arch was analyzed in its unreinforced state, while the second test incorporated strengthening through externally bonded

Carbon Fiber Reinforced Polymer (CFRP) laminates. The appearance of initial tensile-induced cracking in the unreinforced model led to the strategic placement of CFRP in tension-prone zones. The strengthened specimen exhibited significantly enhanced resistance to out-of-plane lateral forces. To simulate the composite mechanical behavior of the masonry comprising both stone units and mortar—an equivalent elastic modulus of 4050 MPa was assigned. For the finite element discretization, the C3D8R 8-node linear brick elements with reduced integration were employed consistently throughout the model [14].

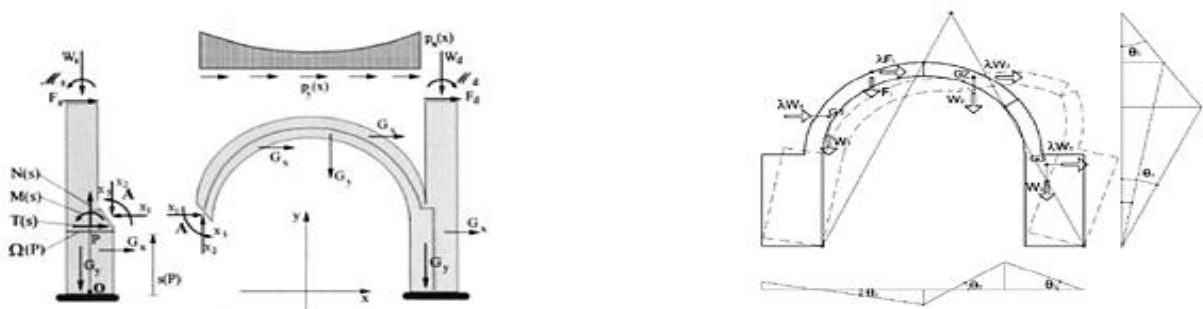


Fig. 9. Arrangements of lateral and radial anchorages in the studied bridge [10]

Figure 10 illustrates the numerical distribution of stress fields within the structural model. As evidenced in Figures 11 and 12, the simulation results obtained in this study exhibit strong agreement with those

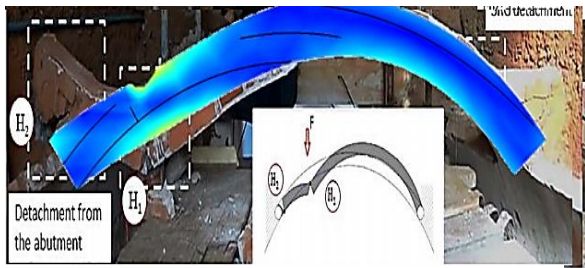


Fig. 10. Stresses in the mode validation

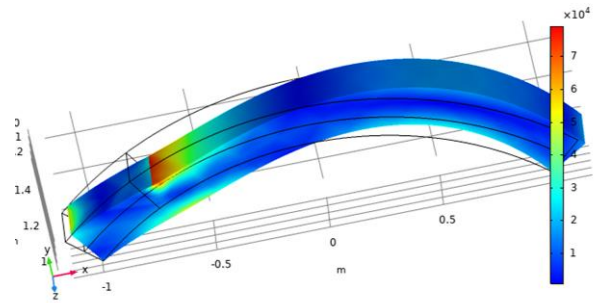


Fig. 11. Arrangement of the curve results

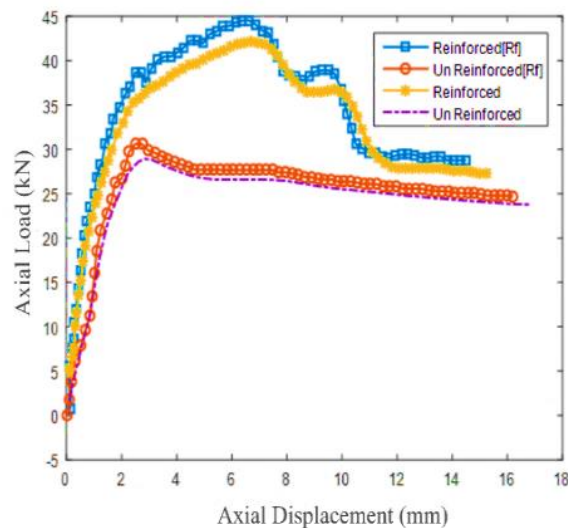


Fig. 12. An analytical comparison between the load–displacement response of the control specimen and the corresponding behavior of the validated model is presented.

3.2 Mesh Size Sensitivity Assessment

To verify the mesh-independency of the finite element results, a sensitivity analysis was carried out on the configuration featuring the maximum arch density, as this scenario is expected to exhibit the highest structural resistance. This configuration was deliberately selected, since its intensified arch layout represents the most demanding

condition in terms of numerical convergence and stiffness response. Demonstrating mesh independence under this critical case supports the validity of the results across all other configurations. Figure 13 illustrates the variation in arch resistance obtained from five distinct meshing schemes.

In the meshing process, C3D8R elements were employed for the arch, while C3D6

elements were utilized for the spandrel wall and cornice components. The meshing was executed using the sweep technique, and the nonlinear dynamic analysis was performed using Abaqus 2020. Due to the fact that the problem is solved using finite element equations under boundary conditions of the pile heads, a highly refined and fine mesh is

required. This necessity arises because the main cause of wave propagation and dynamic response is the pressure differential. If the solution path is based on this pressure gradient, then a much denser mesh must be utilized to capture the variations accurately. The mesh configuration employed in this analysis is illustrated in Figure 14.

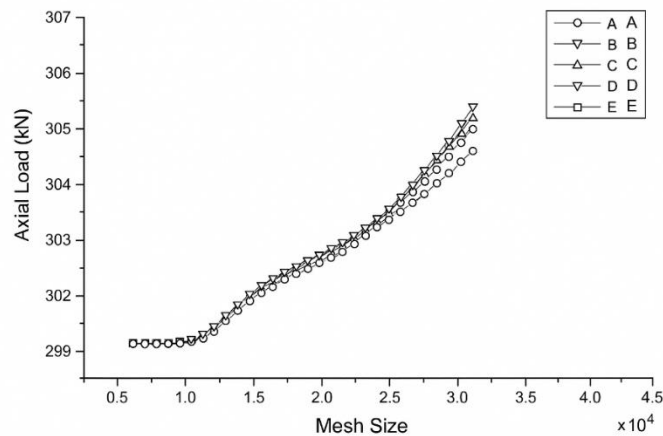


Fig. 13. Comparative Strength Performance of Five Distinct Reinforcement Mesh Arrangements.

Details regarding the nodal distribution across the five distinct configurations, along with the corresponding error percentages, are summarized in Table 6. Notably,

configuration D achieved mesh convergence, exhibiting a discretization error below 0.003%, thereby confirming mesh independence.

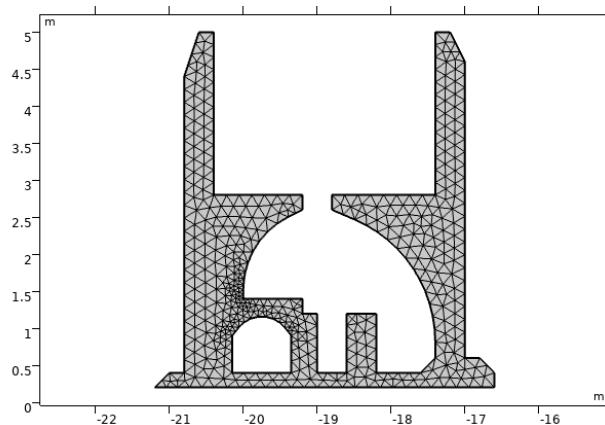


Fig. 14. Type of mesh used in the validation process

Table 6. Number of Nodes and Error Percentage

Mesh	Number of Points	Error Percentage
Mesh A	5000	6.13
Mesh B	10000	4.11
Mesh C	25000	2.37
Mesh D	45000	0.0035
Mesh E	80000	0.0001

4. Result and Discussion

4.1. Numerical Modeling of Arch-Type Vault Structures

4.1.1. Numerical Modeling of the Unretrofitted Masonry Arch

In Figure 15, the windcatcher under investigation is shown with its arched masonry vault. In the numerical modeling process of the unreinforced masonry vault, the geometry was designed based on the traditional form of historical arches. However, to enhance convergence behavior during the numerical solution, certain non-essential geometrical details were deliberately simplified (see Figure 16). The purpose of this simplification was to reduce unnecessary meshing complexity and facilitate the implementation of the finite element analysis. A structured meshing algorithm was employed to generate a high-accuracy mesh.



Fig. 15. The actual vault specimen located on-site

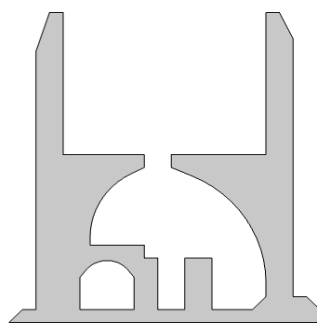


Fig. 16. Unreinforced Arch-Shaped Vault Model (Model A-S-1)

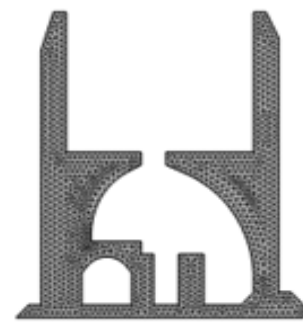


Fig. 17. Unretrofitted Barrel Vault Arch Model (Model A-S-1)

In this approach, mesh refinement was specifically concentrated in regions prone to stress concentration (refer to Figure 17). The mesh type and density were selected based on a validated methodology introduced in a prior benchmark study on numerical model verification. That study compared various meshing configurations and proposed an optimal scheme to improve analysis accuracy. The precise selection of the mesh structure played a pivotal role in enhancing the accuracy of results and reducing the computational time required for numerical convergence.

Figures 18–20 provide critical insights into the structural response of the unreinforced arch

subjected to seismic excitation from the Sarpol-e Zahab earthquake. As illustrated in Figure 18, the stress distribution reveals a

pronounced concentration at the right springing of the arch. This region, characterized by a high slenderness ratio and

diminished effective cross-section, is structurally predisposed to dynamic stress amplification. Furthermore, elevated stress levels were detected at the left side of the crown, which can be attributed to the superimposed effects of gravitational loading and lateral seismic components. In Figure 19, the deformation pattern of Model A-S-1 indicates that the maximum lateral displacement is similarly localized at the right base. The peak displacement, reaching approximately 14 cm, reflects significant inelastic deformation within a structurally critical zone, directly correlating with the identified stress concentrations. Figure 20

displays the distribution of plastic strain throughout the model. The highest strain value, approximately 0.005, was observed in the left column, indicating localized yielding and the onset of nonlinear material behavior. Although the left column is the primary locus of plasticity, the right column also demonstrated notable inelastic response and visible local damage. The concurrent emergence of strain and stress concentrations at opposing supports suggests a complex interaction of failure mechanisms and may signal the early stages of progressive collapse under seismic loading.

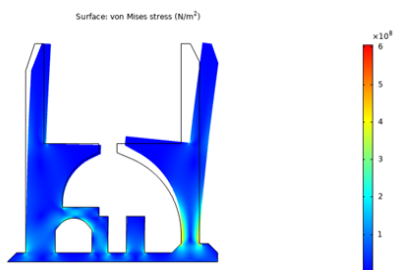


Fig. 18. Stress distribution for model A-S-1

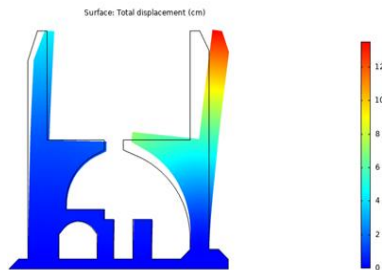


Fig. 19. Maximum Displacement Observed for Model A-S-1

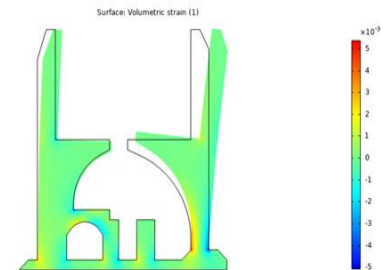


Fig. 20. Plastic Strain Distribution in Model A-S-1

4.1.2. Seismic Retrofitting of Arched Vaults

Based on the results discussed earlier, the highest concentration of strain and damage in the flat arch structure occurs at the right base under seismic excitation, primarily due to asymmetrical dead load distribution. To improve the seismic performance, full-structure retrofitting is therefore recommended. The modeling of steel and FRP reinforcement bars, along with the adopted meshing strategy in ABAQUS, follows the procedures outlined by Norouzi et al. [16] and Wang et al. [17].

4.1.3. Retrofitting Using Near-Surface Mounted (NSM) Steel Reinforcement Bars

Earthquake-induced loads must be considered critical design actions when assessing the

structural behavior of retrofitted elements. The reinforcement detailing must be sufficient to accommodate seismic demands. Figure 21 illustrates the reinforcement configuration of the arch slab element that has been retrofitted using the Near-Surface Mounted (NSM) technique. The arrangement of the steel bars is optimized to resist expected seismic forces while maintaining compatibility with the original structure. In finite element modeling, due to the distinct mechanical properties of steel reinforcements and surrounding concrete, the mesh in the reinforcement zones must be significantly refined to ensure numerical accuracy and convergence. This requirement is primarily governed by the interface (surface-to-surface) boundary

condition, which necessitates a denser mesh to accurately capture the interaction between different materials. Figure 22 displays the mesh distribution applied in model A-S-2, where this refinement approach is evident. In this model, the total number of generated

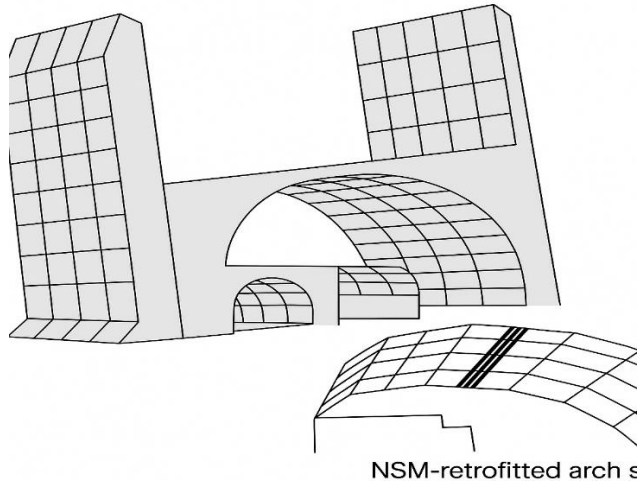


Fig. 21. NSM reinforcement configuration of the arch slab

As illustrated in Figure 23, the stress distribution for model A-S-2 is presented. As discussed in the previous section, the stability of the stress values and their consistency with the initial conditions suggest that the meshing in the base region of the column has been performed with sufficient accuracy. No significant numerical errors were observed in the modeling process. It is important to note that this stress stability stems from the direct relationship between stress and the force-to-area ratio. In this model, both the applied force and the cross-sectional area remained constant; the only addition to the system was reinforcement using steel rebar, which did not affect the overall stress values. Figure 24 illustrates the maximum displacement distribution in model A-S-2. A comparison

elements exceeds one million, which represents an approximate 4.5% increase compared to the unretrofitted configuration, confirming the influence of mesh density in the accuracy of simulation results.

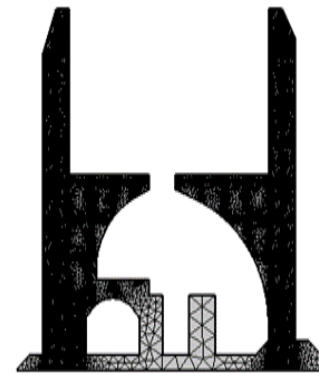


Fig. 22. Mesh discretization in model A-S-2

with the unretrofitted model shows a reduction of approximately 43% in the maximum displacement. This substantial decrease clearly demonstrates the effectiveness of steel rebar reinforcement in enhancing the seismic performance of the structure and reducing deformations under dynamic loading conditions. As shown in Figure 25, the plastic strain contours for model A-S-2 are depicted. The maximum plastic strain in this model reaches approximately 0.003. When compared to the unretrofitted case, this represents a 36% reduction in plastic strain, indicating a notable improvement in the nonlinear behavior of the structure and an increase in the arch's resistance to seismic loads following the retrofitting procedure.

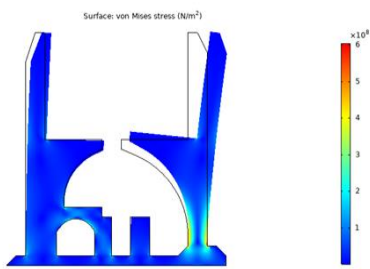


Fig. 23. Stress distribution in model A-S-2

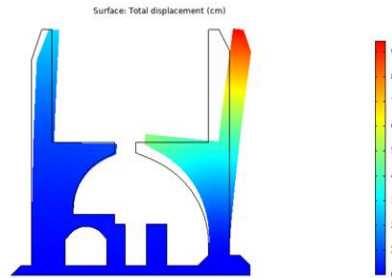


Fig. 24. Maximum displacement distribution in model A-S-2

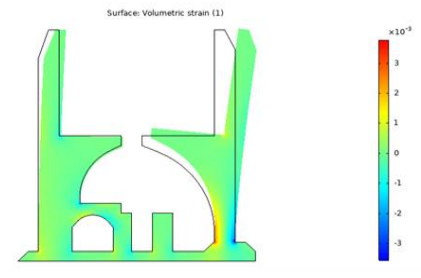


Fig. 25. Plastic strain contours in model A-S-2

4.1.4. Strengthening of Arch Vaults Using FRP Reinforcement Bars

The entire structure was retrofitted using Near-Surface Mounted (NSM) FRP bars with a yield strength of 700 MPa. In the numerical simulation, due to the differing material properties between the FRP bars and the concrete substrate, a denser mesh was applied in the interface regions to ensure convergence and accuracy of the solution. This mesh refinement was necessary to satisfy the boundary conditions associated with the surface-to-surface interaction, commonly referred to as the interface contact behavior. Figure 26 presents the stress contour distribution for the A-S-3 model. As shown, stress concentrations are evident at the base and crown of the arch, indicating the load path redistribution due to the introduced FRP elements. Figure 27 displays the maximum

displacement contour for the A-S-3 model. By comparing this result with the corresponding un-strengthened model, it becomes evident that the application of FRP bars resulted in a displacement reduction of up to 54%. This substantial improvement demonstrates the effectiveness of FRP reinforcement in limiting structural deformations under loading. Figure 28 shows the plastic strain contour for the A-S-3 model. Compared to the un-strengthened model, plastic strain was reduced by approximately 48%, while also showing an 11% improvement relative to the model strengthened using conventional steel bars. The strain distribution pattern indicates tensile strain development on the left side of the vault and compressive strain on the right side, aligning with the expected behavior under lateral or asymmetric loading conditions.

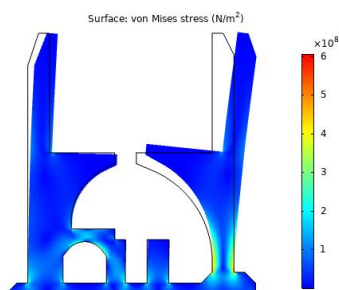


Fig. 26. Stress distribution in model A-S-3

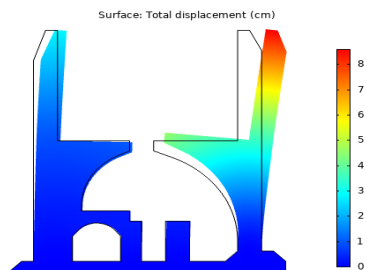


Fig. 27. Maximum displacement distribution in model A-S-3

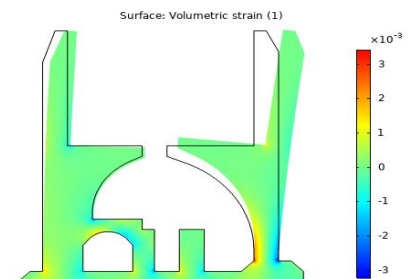


Fig. 28. Plastic strain contours in model A-S-3

4.1.5. Seismic Performance Assessment of Arch Models under the Sarpol-e Zahab Earthquake Record

Figure 29 illustrates the displacement–time response of the diaphragm in model A-S-1 subjected to the Sarpol-e Zahab earthquake record. According to the results, the peak displacement reached approximately 13 cm, which aligns well with the predicted response of the unretrofitted baseline model. This level of agreement reflects the accuracy and reliability of the employed numerical modeling approach. Subsequently, the displacement–time response of model A-S-2, which incorporates steel rebar reinforcement solely at the column bases, was analyzed. The results indicate a notable reduction of approximately 54% in diaphragm displacement due to this retrofitting strategy, thereby demonstrating a substantial enhancement in the system's seismic performance. Furthermore, the time-history responses of the arched configuration reveal a comparative performance evaluation between the unretrofitted system, the FRP-rebar reinforced system, and the steel-rebar reinforced system. The maximum displacement of the arch was reduced by approximately 11% and 43% in the FRP and steel rebar cases, respectively. These significant reductions in seismic response underscore the effectiveness of the adopted retrofitting techniques and further validate the

robustness of the meshing strategy and the numerical simulation method used across other model scenarios.

Figure 30 illustrates the pushover curve of the arch model subjected to the Sarpol-e Zahab earthquake record. As can be seen in this graph, the application of retrofitting techniques has led to a substantial reduction in both base shear and displacement. This reduction has been reported to reach approximately 46%, highlighting the effectiveness of the implemented strengthening methods in improving seismic performance. Table 7 presents the maximum values of stress, displacement, and plastic strain for the studied model. Based on a comparison between the minimum and maximum displacement values, it can be inferred that the structural resistance improved by approximately 45% as a result of the applied retrofitting techniques. To analyze the residual behavior of the specimen, the arch was initially subjected to axial loading, followed by subsequent loading cycles for structural evaluation. For instance, Figure 31 illustrates specimen A-S-1, which exhibited a reduction in the shear capacity of the column after the third loading cycle in the first quadrant and again after the fourth cycle in the third quadrant. This reduction is most likely attributable to the crushing of adobe at the column base, which impaired the structural integrity during cyclic loading.

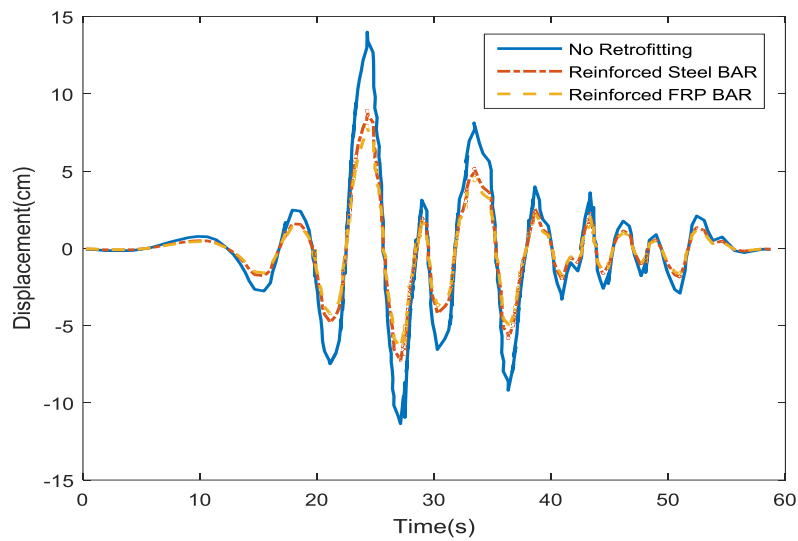


Fig. 29. Displacement–Time Response of the Diaphragm in the Arch Model Subjected to the Sarpol-e Zahab Earthquake Record

Table 7. Maximum Stress, Displacement, and Plastic Strain Results for the Arch Model

Model Name	Maximum Stress (Pa)	Maximum Displacement (cm)	Plastic Strain
A-S-1	6×10^8	14	5.1×10^{-3}
A-S-2	6×10^8	9	5.3×10^{-3}
A-S-3	6×10^8	8	3.1×10^{-3}

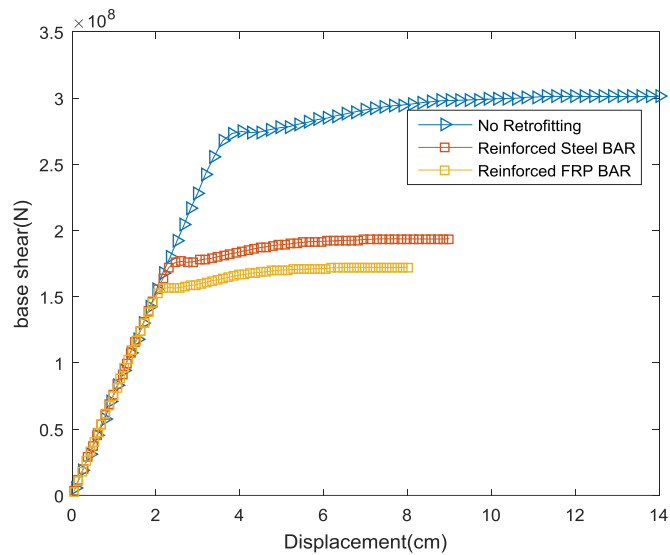


Fig. 30. Pushover Curve of the Arch Model Subjected to the Sarpol-e Zahab Earthquake Record.

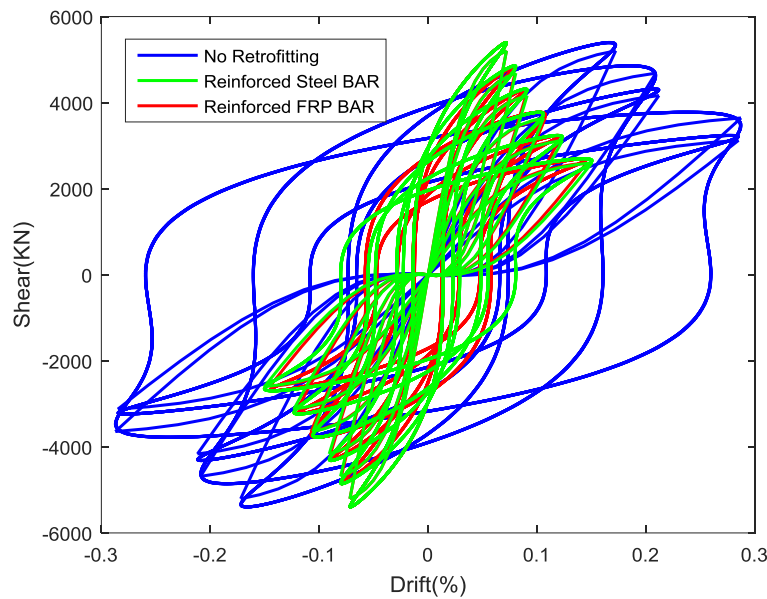


Fig. 31. Hysteresis Curve of the Arched Vault Subjected to the Sarpol-e Zahab Earthquake

4.1.6. Seismic Performance Assessment of Arch Models under the Tabas Earthquake Record

Figure 32 illustrates the displacement–time response diagram of the diaphragm in model A-T-1 subjected to the Tabas earthquake record. In this analytical approach, the structure is exposed to an incremental dynamic excitation, and the maximum structural responses are extracted with respect to time, from the onset of excitation up to any desired time point. These responses are typically considered as the peak absolute values of the dynamic outputs. Depending on the analytical objective, the selected response parameters may involve one or more

structural performance criteria relevant to seismic evaluation and design. In the same figure, the displacement–time diagram of the diaphragm for model A-T-2 under the Tabas earthquake record is also presented. The results obtained for the arch structure in three conditions—unretrofitted, retrofitted with steel rebars, and retrofitted with FRP bars—demonstrate that the maximum displacement of the arch decreased by approximately 13%, 42%, and even further, respectively. This comparison highlights the effectiveness of the retrofitting strategies, particularly those utilizing FRP bars, in significantly mitigating seismic deformations.

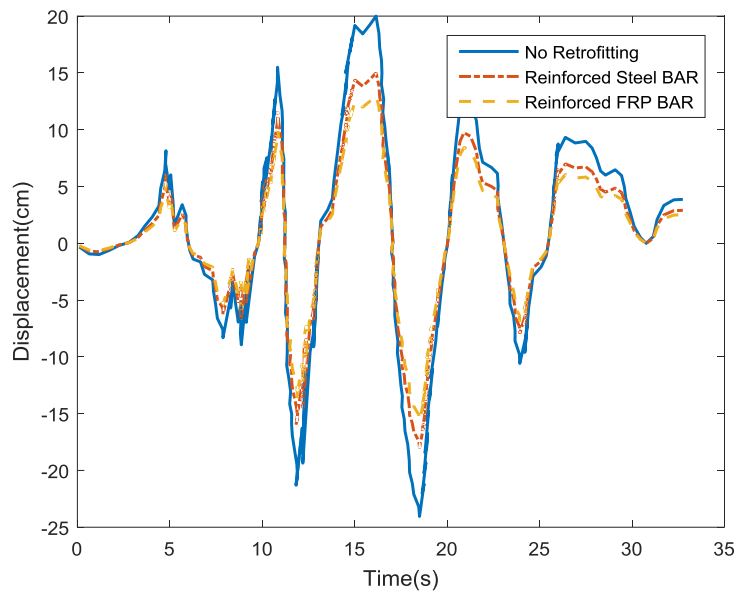


Fig. 32. Diaphragm Displacement–Time Response of the Models under the Tabas Earthquake Record

Figure 33 illustrates the pushover curves of the structural models subjected to the Tabas earthquake record. As previously discussed, the results demonstrate that the reduction in seismic response due to different retrofitting strategies can reach up to 50%. Additionally, compared to the Sarpol-e Zahab earthquake, the Tabas event leads to approximately a 25% increase in base shear demand. This notable difference underscores the influence of

seismic record characteristics on structural performance and must be considered in the seismic design and evaluation of retrofitted systems. Table 8 presents the results for the maximum stress, displacement, and plastic strain obtained from the proposed numerical model. A comparative assessment of the minimum and maximum displacement values indicates an approximate 35% improvement in structural resistance.

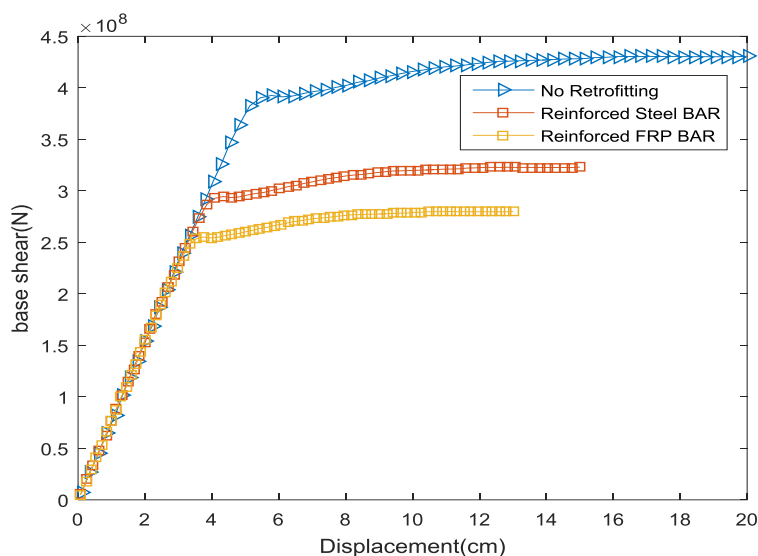


Fig. 33. Pushover Curves of the Models under the Tabas Earthquake Record

Table 8. Maximum Stress, Displacement, and Plastic Strain for the Arch-Shaped Model under Tabas Earthquake

Model Name	Maximum Stress (Pa)	Maximum Displacement (cm)	Plastic Strain
A-T-1	1.7×10^8	20	7.6×10^{-3}
A-T-2	1.7×10^8	15	5.7×10^{-3}
A-T-3	1.7×10^8	30	5.03×10^{-3}

4.1.7. Seismic Performance Evaluation of Arch-Shaped Vault Models under the Northridge Earthquake Record

Figure 34 illustrates the displacement–time response of diaphragm in model A-N-1 subjected to the Northridge earthquake record. Analyzing the results of this plot reveals that the presence of soil–structure interaction (SSI) leads to a reduction in relative displacements. However, due to the increased overall rotation of the structure, a slight increase in absolute displacements is observed.

Another important observation from the analysis is that the lateral displacements are greater when SSI is considered, despite the fact that the lateral force in this condition is lower compared to the non-SSI case. This

phenomenon highlights the significant role of rotation induced by SSI in amplifying the overall displacements of the structure. Moreover, based on the displacement–time diagram for the unretrofitted arch model subjected to the Northridge ground motion, it is observed that the peak displacement in the unretrofitted condition decreases by approximately 13% and 45%, compared to the models retrofitted with FRP bars and steel reinforcement, respectively. These findings indicate the effectiveness of structural retrofitting using composite and steel materials in mitigating the dynamic response of the structure under strong seismic excitation.

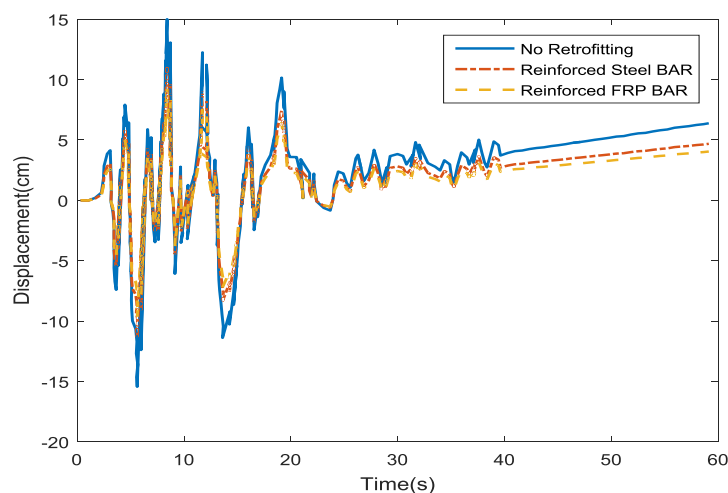


Fig .34. Displacement–Time Response of the Arch-Shaped Vault Subjected to the Northridge Earthquake Record

Figure 35 illustrates the pushover curve of the arched vault subjected to the Northridge

earthquake record. As can be seen, implementing retrofitting techniques has a

significant effect on reducing the base shear force. This reduction indicates an enhanced energy dissipation capacity and improved nonlinear structural performance under seismic excitations. In Figure 36, the hysteresis curve of the structure subjected to

the Northridge ground motion is presented. The results reveal that retrofitting measures lead to a more stable hysteretic behavior, effectively minimizing local instabilities and preventing sudden stiffness degradation throughout the loading cycles.

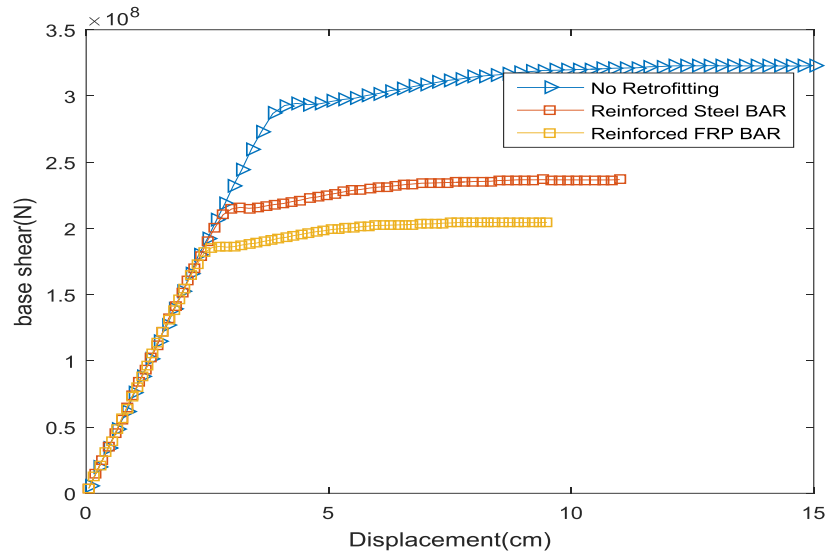


Fig .35. Pushover Curve of Arched Vaults Subjected to the Northridge Earthquake Record

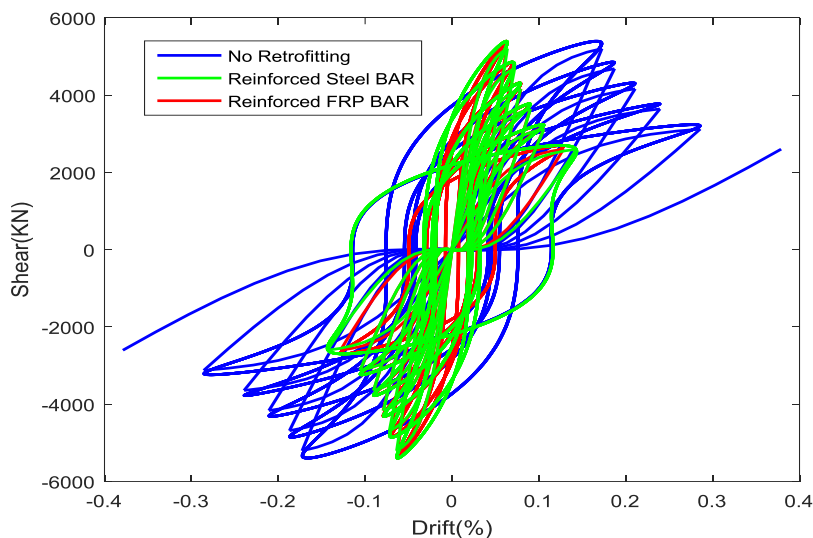


Fig .36. Hysteresis Curve of Arched Vaults Subjected to the Northridge Earthquake

Table 9 presents the results of maximum stress, displacement, and plastic strain observed in the arch-shaped vault subjected to the considered earthquake loading. The comparison between the minimum and maximum displacement values clearly indicates a 35% improvement in structural

resistance due to the applied retrofitting technique. This substantial enhancement highlights the effectiveness of the seismic strengthening approach in reducing deformation and improving the overall performance of the vault structure during seismic excitation.

Table 9. Maximum stress, displacement, and equivalent plastic strain in arch vaults subjected to the Northridge earthquake

Model Name	Maximum Stress (Pa)	Maximum Displacement (cm)	Equivalent Plastic Strain
A-N-1	3.1×10^8	15	5.7×10^{-3}
A-N-2	3.1×10^8	11	4.2×10^{-3}
A-N-3	3.1×10^8	9.5	3.8×10^{-3}

4.2 Comparative Interpretation of Seismic Response

To complement the numerical findings presented earlier, this section provides an in-depth interpretative assessment of how different retrofitting approaches and seismic input characteristics influence the dynamic performance of adobe vault structures. The primary aim is to bridge the quantitative results with structural behavior mechanisms and to extract engineering-level insights that could inform the selection of effective seismic strengthening strategies in practice.

4.2.1 Influence of Retrofitting Method under Uniform Seismic Excitation: The Case of Sarpol-e Zahab

As summarized in Table 7 and illustrated in Figures 23 through 28, the choice of retrofitting material and configuration plays a critical role in governing the structural response of vaults subjected to seismic loading. When subjected to the Sarpol-e Zahab earthquake record, the control model without retrofitting (A-S-1) exhibited the highest deformation demand, reaching a peak lateral displacement of 14 cm and a maximum plastic strain of 5.1×10^{-3} . These results point to a highly nonlinear and damage-prone response under strong ground motion. The model reinforced with conventional steel rebars (A-S-2) demonstrated a notable improvement in seismic behavior, achieving a 43% reduction in peak displacement and a

36% decrease in plastic strain relative to the unretrofitted configuration. Even more significant, however, was the performance of the vault retrofitted with Fiber Reinforced Polymer (FRP) rebars (A-S-3), which achieved a 54% reduction in displacement and a 48% reduction in plastic strain. It is important to note that the maximum stress values remained relatively stable at approximately 6×10^8 Pa across all three models, indicating that while the retrofitting techniques did not affect the global force demand, they considerably enhanced the ductility and energy dissipation capacity of the system. This distinction underscores the effectiveness of FRP as a material particularly suited for seismic applications in historic masonry vaults.

4.2.2 Integrated Comparison of Seismic Displacement Across All Vault Models

Figure 37 illustrates a consolidated bar chart summarizing the peak lateral displacements (expressed in centimeters) recorded for each vault configuration—unretrofitted, steel-reinforced, and FRP-reinforced—when subjected to three distinct seismic inputs: Sarpol-e Zahab, Tabas, and Northridge. This comparative visualization enables a holistic assessment of structural performance by capturing the influence of both the retrofitting strategy and the nature of the earthquake excitation. The figure reveals a consistent trend of reduced displacements across all retrofitted models, with the FRP-reinforced configurations demonstrating the highest

levels of seismic resilience. In contrast, unretrofitted vaults exhibited the most significant deformation demands, particularly under the Tabas earthquake, which imposed the most severe loading conditions due to its high peak ground velocity and prolonged strong-motion duration. The X-axis categorizes the individual vault models (from A-S-1 to A-N-3), while the Y-axis quantifies

the corresponding displacement response. By integrating data across all scenarios, this chart serves as a concise yet powerful decision-making tool, offering engineers and researchers a clear visualization of how different reinforcement strategies and earthquake characteristics collectively impact the seismic performance of historic earthen vault structures.

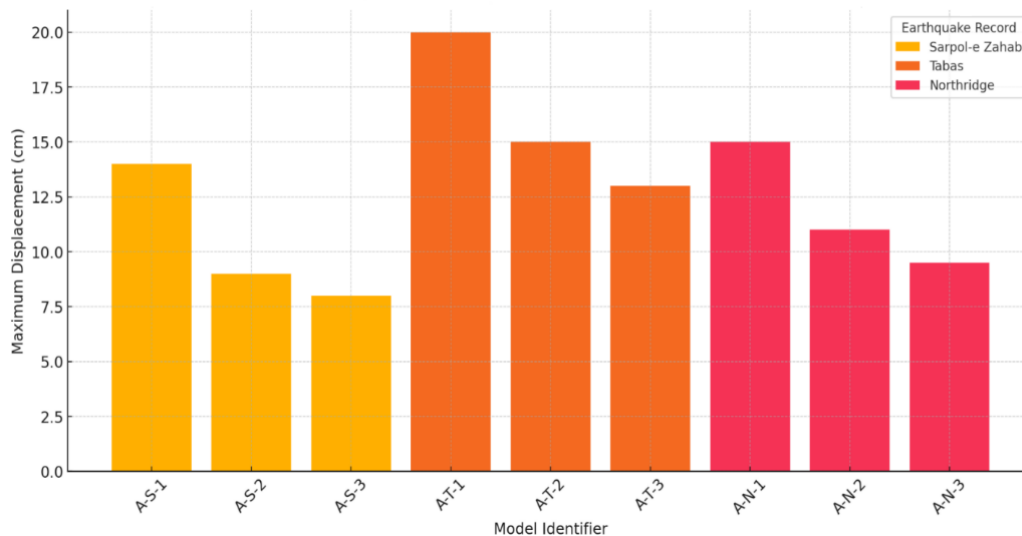


Fig .37. Figure 36. Maximum Displacement Comparison of Vault Models Under Different Earthquake Records

4.2.4 Consolidated Overview of Structural Performance Improvements

Table 10 provides a synthesized overview of the relative improvements in seismic response achieved through retrofitting, expressed as percentage reductions in both peak lateral displacement and equivalent plastic strain, when compared against their respective unreinforced benchmarks. These values are directly derived from the numerical analyses presented in Tables 7 through 9 and offer quantifiable evidence supporting the efficacy of both steel and Fiber Reinforced Polymer (FRP) reinforcement strategies. The data reveal consistent trends across all earthquake

scenarios, confirming that both forms of retrofitting contribute to enhanced structural resilience. Notably, CFRP reinforcement demonstrates superior performance in minimizing deformation demands and controlling plastic behavior, particularly under strong ground motion conditions. These observations are well-aligned with prior findings reported in the literature, including those by Hu et al. (2018), Dimitri & Trentinabin (2020), and Pouraminian et al. (2023), which similarly highlight the advantages of composite-based retrofitting systems for improving the seismic robustness of historic masonry and adobe vault structures.

Table 10. Percent Reduction in Maximum Displacement and Plastic Strain for Retrofitted Vault Models Compared to Unretrofitted Cases Under Different Earthquake Records

Earthquake Record	Model	Retrofitting Type	Displacement Reduction (%)	Plastic Strain Reduction (%)
Sarpol-e Zahab	A-S-2	Steel	43%	36%
Sarpol-e Zahab	A-S-3	CFRP	54%	48%
Tabas	A-T-2	Steel	25%	26%
Tabas	A-T-3	CFRP	33%	34%
Northridge	A-N-2	Steel	27%	26%
Northridge	A-N-3	CFRP	36%	33%

5. Conclusion

This research delivered an in-depth seismic performance assessment of traditional arched adobe windcatcher structures (*Āsbaads*) of Sistan, located in Qaleh Machi, Iran. Utilizing nonlinear time-history analyses and calibrated finite element models built in ABAQUS, the study examined both unstrengthened and retrofitted configurations under three representative earthquake records: Sarpol-e Zahab, Tabas, and Northridge. Two retrofitting strategies were evaluated: conventional steel bars and Fiber Reinforced Polymer (FRP) bars applied through the Near-Surface Mounted (NSM) method. The findings underscored the notable advantages of FRP reinforcement in enhancing ductility, limiting deformation, and increasing energy dissipation capacity without compromising the structural coherence of these heritage adobe systems.

The main conclusions of the study are as follows:

1. Vaults retrofitted with FRP bars consistently exhibited superior performance compared to both unreinforced and steel-reinforced models, achieving up to 54% reduction in peak displacement and 48% reduction in plastic strain.
2. The Tabas earthquake, characterized by high peak ground velocity (PGV) and extended strong motion duration, imposed the most demanding loading scenario across all vault models, particularly affecting unretrofitted configurations.
3. Pushover and hysteresis analyses revealed that FRP reinforcement significantly improved ductile behavior and delayed stiffness degradation—both critical factors in ensuring the seismic resilience of historical structures.
4. The integration of FRP rebars was shown to be effective in preserving load path stability and in mitigating inelastic failure mechanisms under severe cyclic excitations.
5. A comparative chart of maximum displacements, along with a quantitative summary of structural improvements, validated the overall efficiency of FRP retrofitting under all examined seismic conditions.

In summary, this study contributes to the growing body of research supporting the application of advanced composite retrofitting solutions for protecting earthquake-prone historic adobe structures. The results advocate for the use of FRP bars as a preferred seismic

rehabilitation technique in traditional vault constructions, providing both technical

6. References

- [1] Button, M. R., Cronin, C. J., & Mayes, R. L. (2002). Effect of vertical motions on seismic response of highway bridges. *Journal of Structural Engineering*, 128(12), 1551–1564. [https://doi.org/10.1061/\(ASCE\)0733-9445\(2002\)128:12\(1551\)](https://doi.org/10.1061/(ASCE)0733-9445(2002)128:12(1551))
- [2] Hoo, C. P., Gergely, J., & L. D. (2007). In-situ verification of rehabilitation and repair of reinforced concrete bridge bents under simulated seismic loads. *Earthquake Spectra*, 17(3), 507–530.
- [3] Garmeh, V., Nikghalb Rashti, A. A., Adibramezani, M., Hojat Kashani, A., & Adibi, M. (2022). SMA-based self-centering eccentrically braced frame with vertical link member. *Structures*, 43, 1230–1258. <https://doi.org/10.1016/j.istruc.2022.07.034>
- [4] Arezoomand Langarudi, P., Adibramezani, M., Hojatkashani, A. *et al.* Effect of Design Optimality and Overstrength on the Seismic Performance of Steel Plate Shear Walls. *Iran J Sci Technol Trans Civ Eng* 49, 1401–1419 (2025). <https://doi.org/10.1007/s40996-024-01513-7>.
- [5] Arezoomand, P., Khodadadi, R., & Shafiei, H. (2025). Comparison of Median Collapse Capacity of Steel Plate Shear Walls Using Approximate (Pushover-to-Fragility) and Exact Methods. *Journal of Structural and Construction Engineering*, 51(1), 33–47. [10.22065/jsce.2025.470572.3482](https://doi.org/10.22065/jsce.2025.470572.3482)
- [6] Tutankhamun, P., Oshima, T., Balagoru, S., & Yamazaki, T. (2010). Ferro cement jacketing for retrofitting of reinforced concrete bridge piers for enhanced shear strength. In 2nd Int. Workshop on Structural efficacy and cultural preservation value for vulnerable architectural heritage.
- Health Monitoring of Innovative Civil Engineering Structures (SHM ISIS), Canada.
- [7] Boury, A., Castori, G., & Corradi, M. (2011). Intrados strengthening of brick masonry arches with composite materials. *Composites Part B: Engineering*, 42(5), 1164–1172. <https://doi.org/10.1016/j.compositesb.2011.03.005>
- [8] Dimitri, R., & Tornabene, F. (2015). A parametric investigation of the seismic capacity for masonry arches and portals of different shapes. *Engineering Failure Analysis*, 52, 1–34. <https://doi.org/10.1016/j.engfailanal.2015.02.021>
- [9] Carozzi, F., Poggi, C., Bertolesi, E., & Milani, G. (2018). Ancient masonry arches and vaults strengthened with TRM, SRG and FRP composites: Experimental evaluation. *Composite Structures*, 187, 466–480. <https://doi.org/10.1016/j.compstruct.2017.12.075>
- [10] Button, H., Cronin, X., & Ye, J. (2020). Fire resistance performance of FRP rebar reinforced concrete columns. *International Journal of Concrete Structures and Materials*, 3(2), 111–117.
- [11] Pouraminian, M. (2022). Multi-hazard reliability assessment of historical brick minarets. *Journal of Building Pathology and Rehabilitation*, 7(1), Article 10. <https://doi.org/10.1007/s41024-021-00148-9>
- [12] Cachim, P. B. (2009). Mechanical properties of brick aggregate concrete. *Construction and Building Materials*, 23(3), 1292–1297. <https://doi.org/10.1016/j.conbuildmat.2008.07.023>

[13] Moslehi Tabar, A., & Najafi Dehkordi, H. (2018). Transverse vibration analysis of complicated truss arch bridges using continuum elements. *Amirkabir Journal of Civil Engineering*, 50(1), 53–60.

DOI: 10.22060/ceej.2017.10876.4943

[14] Seyedsjadi, S. M. (2019). Natural environment and ancient monuments of Sistan plain. *Journal of Geographical Research*, 56–57, 146–186.

[15] Akbarzadeh Morshedi, A., & Panahi, F. T. (2020). Experimental investigation of the behavior of brick masonry arches (vault and rib cover) unreinforced and reinforced with C-FRP under simultaneous vertical and horizontal loads. *Advanced Research in Civil Engineering*, 2(3), 41–50.

10.30469/arce.2020.117872

[16] Noroozi, F., Kalate, F., & Lotfollahi Yaghin, M. A. (2016). Numerical analysis of the dynamic behavior of a weighted concrete dam under the explosive load inside the tank. *Journal of Civil and Environmental Engineering*, 47(86).

[17] Wang, H., Zha, X., & Ye, J. (2009). Fire resistance performance of FRP rebar reinforced concrete columns. *International Journal of Concrete Structures and Materials*, 3(2), 111–117.

DOI 10.4334/IJCSM.2009.3.2.111